

## Numerical simulation of ice fracture by compression using of the discrete element method

D.V. Grinevich  , V.M. Buznik, G.A. Nyzhnyi

Federal State Unitary Enterprise All-Russian Scientific Research Institute of Aviation Materials State Research  
Center of the Russian Federation, Moscow, Russia

✉ [d.v.grinevich@gmail.com](mailto:d.v.grinevich@gmail.com)

**Abstract.** The article provides numerical simulation of ice fracture by compression using of the discrete element method by the software Yade. The Bonded Particle Model with damage was used. The computational calibration of the material parameters was performed on the test model of the sample in the form of a hyperboloid, the difference in strength by tensile and compression was 3.26 times. A comparison of real and computational tests on compression of cylindrical samples with diameter and height 50 mm at a temperature of -10 °C was carried out. The deformation curves are similar in the general character, reactions level, and deformations. The method makes it possible to simulate the ice fracture. According to the estimation of the deformation work, the difference between the typical experimental curve and the calculated is about 2 %.

**Keywords:** ice, fracture, damage, discrete element method, bonded particle model

**Acknowledgements.** Research was conducted under the support of the Russian Science Foundation, Grant no. 18-13-00392.

**Citation:** Grinevich DV, Buznik VM, Nyzhnyi GA. Numerical simulation of ice fracture by compression using of the discrete element method. *Materials Physics and Mechanics*. 2023;51(3): 75-87. DOI: 10.18149/MPM.5132023\_10.

### Introduction

Knowledge of the mechanical properties of ice can provide insights into its impact on ships, bridge supports or offshore platforms, as well as the applications of ice a structural material to build infrastructure in regions with a cold climate: roads, runways, loading docks, and others. It is especially important to study the behavior of ice during compression, for which it has the greatest strength [1]. Modern studies on the mechanical properties of ice have largely focused on dynamic loading of ice [2–8]. To predict the behavior of ice-based structures, modeling is performed using various numerical methods. A review of the methods used for such modeling is carried out in our earlier study [9]. Methods for ice modeling can be categorized into phenomenological, mesh-based and meshless methods.

Phenomenological methods provide a general description of the object considered. In this case, only the phenomenon is described, and detailed study of the internal mechanics of the object is unnecessary. Consequently, the internal mechanics of the process is not fully taken into account [10].

Mesh-based methods for modeling problems of ice mechanics are assessed in [11]. A proven mesh-based method for continuum mechanics is the finite element method (FEM). The complex process of nonlinear deformation and brittle fracture in a material should be

simulated using extended models, including nonlinear FEM models of isotropic materials developed by Johnson and Holmquist, Lemaitre, etc. FEM has the following drawbacks: if the models have different scales, the solution is unstable against variation in model parameters (producing a non-convergent solution), considerable additional costs for validating the models are required to determine the parameters (especially for the Johnson–Holmquist model). It is complicated to apply FEM to solving brittle fracture problems, since it is adapted to solutions for continuum media: this is associated with the known problems of mesh-based methods, with mesh distortions appearing under large strain, erosion of elements, and consequent mass and energy losses.

It is concluded in [11] that meshless methods are preferable for solving problems of ice mechanics.

Smoothed-particle hydrodynamics (SPM) is a meshless method replacing the medium by a set of particles. The parameters of the medium are distributed to this system of particles, i.e., "smoothed out" between them. The method allows to simulate large strains and fracture in the medium by separating particle aggregates [10]. It is often necessary to correct the model to eliminate unsteady oscillatory processes in particles; this aspect of the method can introduce non-physical effects into the deformation of solids [12–13].

The discrete element method (DEM) constructs models of solids from individual elements connected by virtual bonds. This method is well adapted to describing rapid processes associated with transfer of matter. The physical state of the continuum medium in DEM consists of the physical states of a large number of individual elements, its macroscopic state is the result of their interaction. The method was developed to simulate molecular dynamics of particles [14], and was later adapted to studying the dynamics of rocks [15] and granular assemblies [16]. DEM is well suited for describing the dynamics of rapid failure processes. A particularly noteworthy model of bonded particles is constructed using additional virtual bonded beams. This approach allows modeling bulk solids. Various types of DEM software implement the model of bonded particles, for example, EDEM [17], LIGGGHTS [18], MercuryDPM [19], Yade [20], Pasimodo [21]. Yade software was used in this study. This system incorporates a damage model for setting the bonds between the elements. Yade is distributed under an open license, with open source code for building discrete numerical models, the solver is written in C++. Preprocessing (building the model, setting the properties and boundary conditions, setting the solver parameters, controlling the solver), as well as postprocessing (output and processing of results) are carried out via Python scripts.

### Experimental study of ice compression

The experimental study of ice compression was carried out for cylindrical specimens. Five specimens were tested to obtain the data. Figure 1(a) shows a specimen placed in a testing machine. Ice specimens were made from distilled water, which was poured into cylindrical metal molds measuring  $\varnothing 50 \times 50$  mm. The specimens were frozen at a temperature of  $-18$  °C. The edges of the cylinder were aligned to be parallel after freezing.

The tests were carried out at a temperature of  $-10$  °C on an electromechanical machine in a thermal cryochamber using a freon mixture as a cooling agent. The specimens in a free state were subjected to compression with steel plates 100 mm in diameter.

The strain of the specimen  $\varepsilon$  was determined as the ratio of the displacement of the compression plate to the initial height of the specimen:

$$\varepsilon = \frac{u}{h}, \quad (1)$$

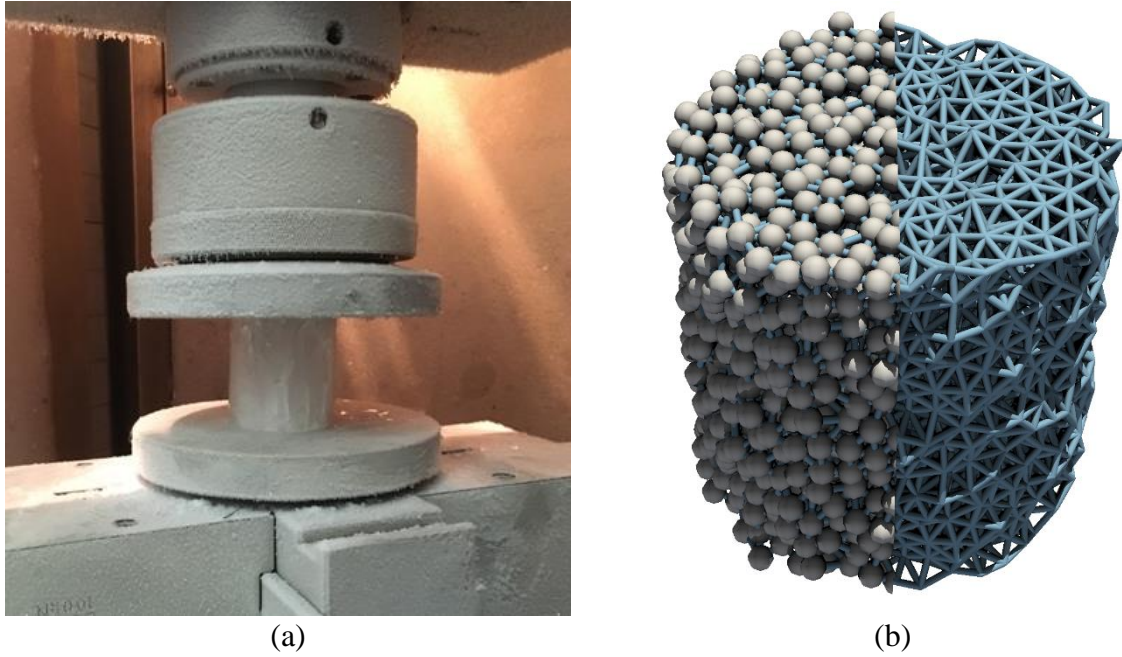
where  $u$  is the plate displacement,  $h$  is the initial height of the specimen.

The stress  $\sigma$  was calculated as the ratio of the impact force to the initial cross-sectional area of the specimen:

$$\sigma = \frac{F}{A} = \frac{4F}{\pi d^2}, \quad (2)$$

where  $A$  is the area of the initial section of the specimen,  $d$  is the diameter of the initial section of the specimen,  $F$  is the force acting on the specimen.

The stress-strain curve  $\sigma(\varepsilon)$  was then constructed from the ratio of strains and stresses. The computational curve for the deformation of the specimen was constructed similarly for comparison.



**Fig. 1.** Cylindrical ice specimen: placed in a testing machine (a), model of bound particles (b)

### Computational study of ice compression

The computational study of ice compression followed the algorithm of the experiment carried out. Let us consider the main relations for the computational model.

The cylindrical volume was filled with spherical discrete elements of a given diameter in random order (Fig. 1(b)). Unlike other software (for example, EDEM), where the first modeling stage is resource-intensive simulation, where a limiting volume is virtually filled with particles, Yade PC includes a convenient algorithm for "packing" elements with the specified parameters.

The elements were connected by virtual bonded beams connecting the centers of adjacent spheres. Figure 1(b) shows discrete elements (displayed for half of the specimen model for better illustration) and virtual bonds of the elements for the entire specimen volume.

The model of the specimen was located between two absolutely rigid surfaces: the lower one was fixed, the upper one was moving down.

The motion of a single particle  $i$  with mass  $m_i$ , inertia  $\vec{I}_i$ , position in space  $\vec{x}_i$ , with the angular velocity  $\vec{\omega}_i$  under the action of external forces  $\vec{F}_{ij}$  and external moments  $\vec{M}_{ij}$  is calculated from the corresponding Newton and Euler equations:

$$m_i \ddot{\vec{x}}_i = \sum_{j=0}^n \vec{F}_{ij}, \quad (3)$$

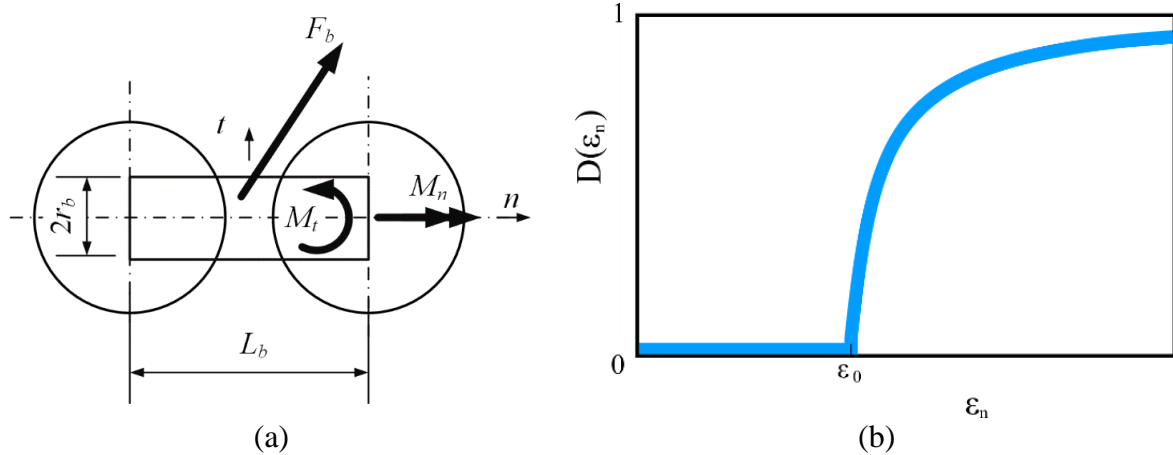
$$\vec{I}_i \dot{\vec{\omega}}_i + \vec{\omega}_i \times \vec{I}_i \cdot \vec{\omega}_i = \sum_{j=0}^n \vec{M}_{ij}. \quad (4)$$

The bond between the particles is a virtual beam that restricts the tangential  $t$  and normal  $n$  displacement of the particles relative to each other (Fig. 2(a)). The forces and moments of the bond reaction are calculated by the following formulas:

$$\begin{aligned}\delta F_n &= -v_n S_n A \delta t; \\ \delta F_t &= -v_t S_t A \delta t; \\ \delta M_n &= -\omega_n S_t J \delta t; \\ \delta M_t &= -\omega_t S_n \frac{J}{2} \delta t,\end{aligned}\tag{5}$$

where  $F_n$ ,  $F_t$  are the projections of the resulting force  $F_b$  in the directions  $n$  and  $t$ ;  $M_n$  is the normal moment;  $M_t$  is the shear moment;  $A = \pi r_b^2$  is the cross-sectional area;  $r_b$  is the radius of rigid coupling;  $J = \frac{1}{2} \pi r_b^4$  is cross-sectional moment of inertia;  $\delta t$  is the time step;  $S_n$  and  $S_t$  are the stiffnesses in the normal and transverse directions;  $v_n$ ,  $v_t$  are the velocities in the directions  $n$  and  $t$ ;  $\omega_n$ ,  $\omega_t$  are the angular velocities around the corresponding axes  $n$  and  $t$ .

The bonds are linear in the simplest formulation of the problem, the bonds break when the yield stresses are exceeded (for example, this is how the model of bonded particles is implemented in EDEM). YAade uses a more complex bond model, developed to simulate fracture mechanics in concrete. The model accumulates damage depending on the strain magnitude during loading. The amount of damage to the material is characterized by the variable  $D$  equal to 0 for undamaged material and 1 for completely destroyed material. This technique allows to simulate different types of complex fracture under compressive and tensile stresses.



**Fig. 2.** Beam bond of particles: scheme of two bonded elements (a), damage function of bonded beams (b)

The ratio of normal stress  $\sigma_n$  and strain  $\epsilon_n$  taking into account damage is written as:

$$\sigma_n = (1 - D \cdot H(\epsilon_n)) \cdot k_n \cdot \epsilon_n,\tag{6}$$

where  $k_n$  is the normal elastic modulus of the bond,  $D \in [0, 1]$  is the damage variable of the material,  $H(\epsilon_n)$  is the Heaviside function excluding the effect of damage during compression (upon crack closure).

The damage variable of the material is determined in terms of the evolutionary function (Fig. 2(b)):

$$D = g(\kappa) = 1 - \frac{\epsilon_f}{\kappa} \exp\left(-\frac{\kappa - \epsilon_0}{\epsilon_f}\right),\tag{7}$$

where  $\kappa = \max \tilde{\varepsilon}$ ,  $\tilde{\varepsilon} = \sqrt{(\varepsilon_n)^2 + \xi_1^2 \cdot |\varepsilon_t|^2}$  is the equivalent stress accounting for damage,  $\xi_1$  is the weight coefficient of the contribution from shear stresses  $\varepsilon_t$ ,  $\varepsilon_0$  is the ultimate elastic strain,  $\varepsilon_f$  is a parameter defined as the intersection of the strain axis and the tangent to the softening curve (characterizes the slope of the softening curve).

Shear stresses are determined by the formula:

$$\tau_t = k_t \cdot \varepsilon_t, \quad (8)$$

where  $k_t$  is the shear elastic modulus of the bond (calculated with respect to  $k_n$  in terms of Poisson's ratio of the bond),  $\varepsilon_t$  is the shear strain.

After virtual bonds are broken, discrete elements interact as independent solids. A full description of the model is given in [20]. Yade constructs the model in a limited volume for commercial reasons, without taking into account the strain rates and ductility; however, it is sufficient for the purposes of our study.

### Determining the parameters of the mathematical model of the material

The strain and compressive fracture of the specimen are calculated by determining the mathematical model parameters of the material (including the functions of bond damage).

The applied model is determined by the following characteristics: the density of discrete elements  $\rho$ , the elastic modulus of element bonds  $k_n$ , Poisson's ratio of element bonds  $\mu$ , the cohesion  $c_0$ , the angle of internal friction  $\varphi$ , the ultimate elastic strain  $\varepsilon_0$ , the relative ductility  $\varepsilon_0/\varepsilon_f$ .

Let us find these parameters. The density of the elements is selected depending on the packing porosity. The density of ice is  $900 \text{ kg/m}^3$ , the density of the elements varies depending on their size to ensure the required mass of the specimen. The dependence of the required particle density on the element size for the given model can be represented as a linear function:

$$\rho(r) = a \cdot r + b, \quad (9)$$

where the coefficients of the equation have the values:  $a = 276 \text{ 742 kg/m}^2$ ,  $b = 1733.6 \text{ kg/m}^3$ .

The element size affects the overall dimension of the problem: a small size significantly increases the number of elements and the computational time.

The macroscopic modulus  $E$  of the specimen material is related to bond stiffness  $k_n$ , the overall slope of the stress-strain curve depends on many factors: the distribution of bonds, their orientation, the magnitude of damage accumulated in them. Therefore, the modulus was ultimately adjusted based on comparing the resulting stress-strain curve with the experimental one. The elastic modulus of the bonds for elements with a radius of 1.5 mm was 1.8 GPa.

The cohesion value  $c_0$  corresponds to critical shear stresses in the absence of normal stresses in the bonds. It was calculated by the formula depending on the angle of internal friction  $\varphi$  and the maximum normal strain [22]:

$$c_0 = k_n \varepsilon_0 \cdot \tan \varphi. \quad (10)$$

Macroscopic Poisson's ratio for ice amounts to  $\mu_{\text{ice}} = 0.344$  [23–24]. Poisson's ratio for bonds was  $\mu$  tailored from a series of computations and is equal to 0.65.

The angle of internal friction for ice is about  $6^\circ$  according to [24–28], which is consistent with our own shearing tests. The ultimate elastic strain was estimated based on the bending failure tests in the tensile region of the specimen [29]. It was found that the mean value is about  $\varepsilon_0 = 0.001 \text{ m/m}$ .

The relative ductility  $\varepsilon_0/\varepsilon_f$  cannot be less than 1 in the model; a slightly higher value (1.1) was taken to ensure brittle fracture during the tensile tests of ice. An increase in this characteristic leads to a more viscous fracture, especially during the tensile tests.

### **Test computations of hyperboloid fracture under uniaxial loading**

Before computations of a specific experiment for compressive fracture of an ice specimen, we conduct test computations allowing to assess a certain model of the material.

The nature of fracture in the model was assessed under uniaxial loading of the hyperboloidal specimen, with stress concentration in its central zone. The problem statement was taken from [16], where it was used to calibrate a model of concrete.

The thinned neck is the region where the body is weakened and the stresses are concentrated, allowing to localize the fracture site. The length of the specimen is taken equal to 100 mm, its maximum diameter is half the length, and the radius of the central section of the hyperboloid is 4/5 of the radius of the extreme section.

Computations for tension and compression of the specimen were performed separately. Table 1 presents the computational results for fracture of the hyperboloid: the upper row shows a stress-strain curve for both compression and tension (two independent computations).

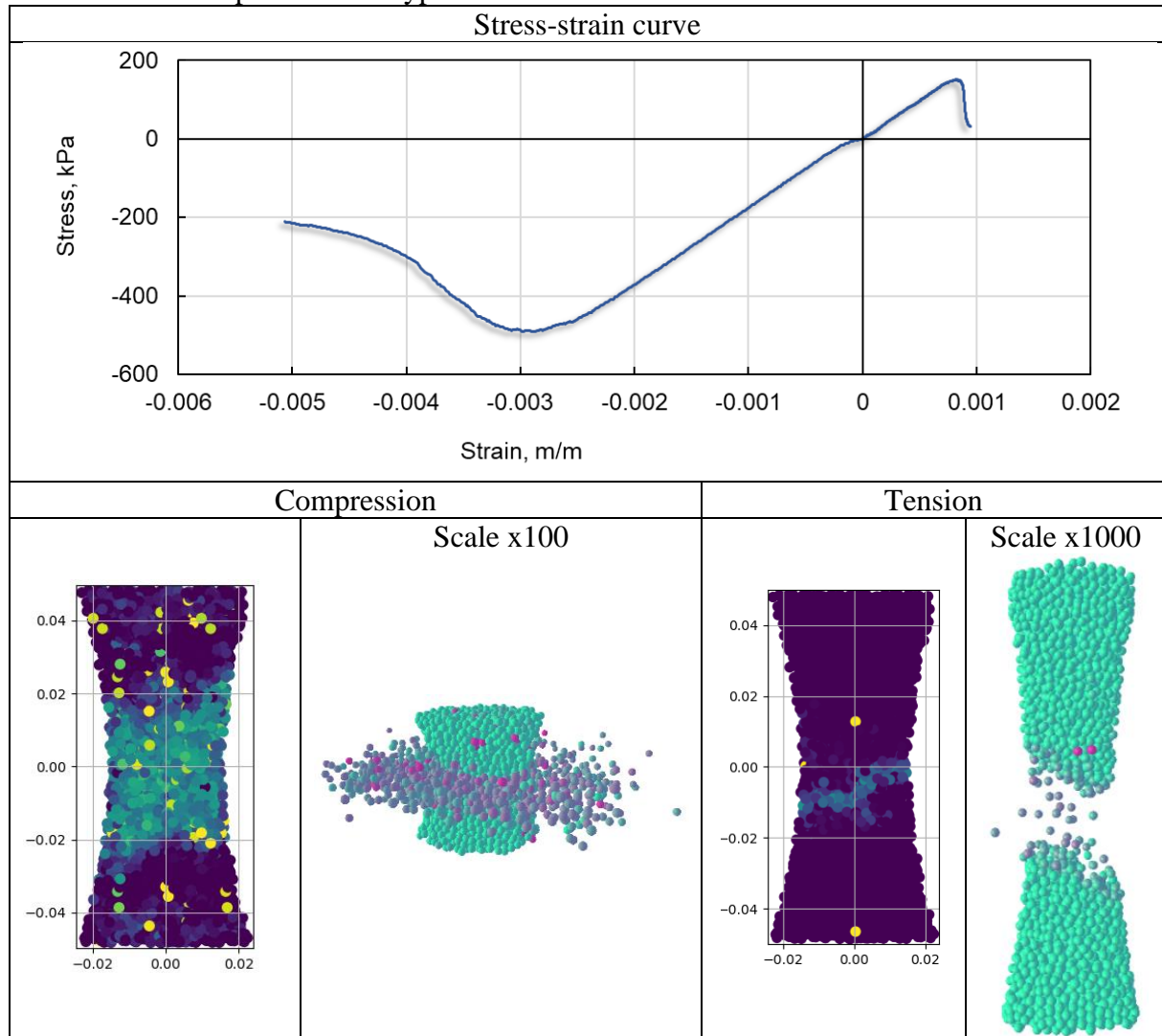
The bottom row shows visualization of the model at the time of fracture.

Two-dimensional projections are given with the sizes, the coordinates are plotted in meters. The magnitude of accumulated damage is shown on a color scale going from dark to light colors: purple corresponds to undamaged material  $D = 0$  (all bonds between elements are intact), yellow to fractured,  $D = 1$  (all bonds between elements are destroyed), intermediate values are shown in green.

The corresponding 3D visualizations of the models at the time of fracture are also given. The displacements of discrete elements in these visualizations are shown with an x100 magnification for compression and with an x1000 magnification for tension. The magnitude of accumulated damage is shown in different colors: light green corresponds to undamaged material,  $D = 0$ , bright pink to fractured  $D = 1$ .

Compressive strength is 3.26 times greater than tensile strength. Tensile fracture is brittle, localized in a small central region. Cracking occurs in the central region during compression, the stress-strain curve has a flat slope, with a gradual decrease in strength after passing the peak, corresponding to the fragmentation of the fractured material. The model illustrates the physical nature of fracture in ice (Table 1).

**Table 1.** Test computations of hyperboloid fracture

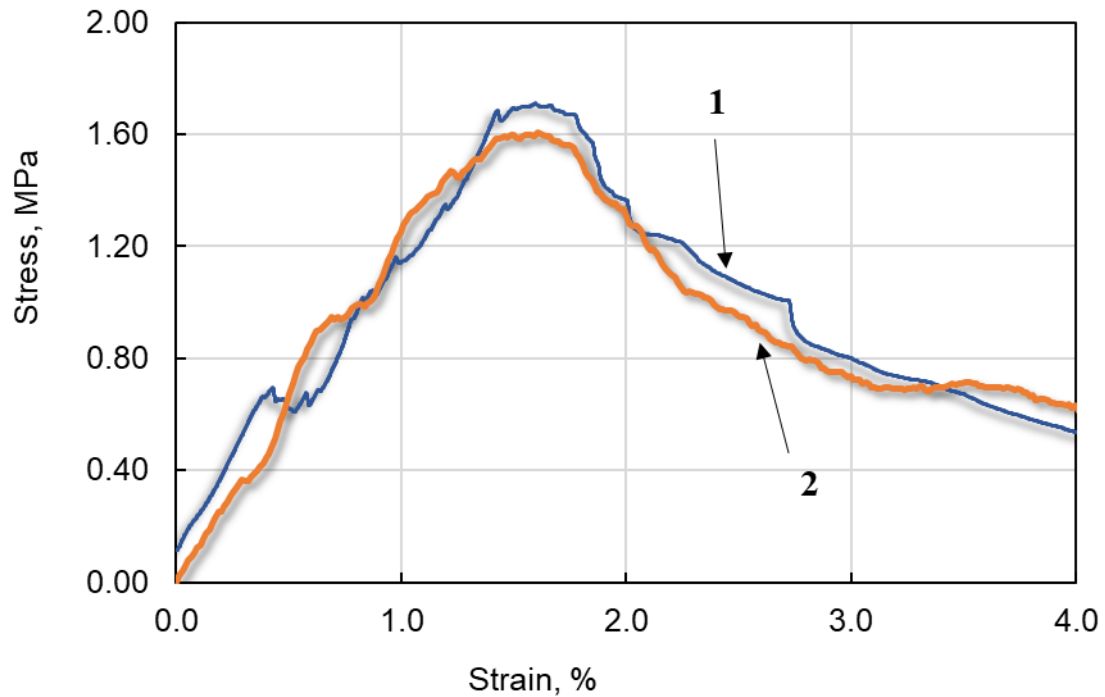


**Results and discussion**

After the test computations were performed and the model parameters were calibrated, compressive fracture was simulated for the cylindrical specimen. Experimental data are given in detail in [1].

Figure 3 shows the resulting stress-strain curves: typical experimental curve (1) and resulting computational curve (2). Local small peaks on the curve correspond to cracking of the material.

The stress-strain curves show a similar behavior. The model physically describes the loading and fracture of the ice specimen. The level of load and strain is in agreement with the experimental results. The difference between the experimental and computational strain values for compression of the ice specimen was about 2%.



**Fig. 3.** Stress-strain curves: typical experimental curve (1) and computational curve (2)


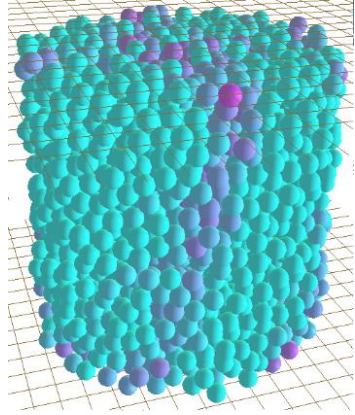

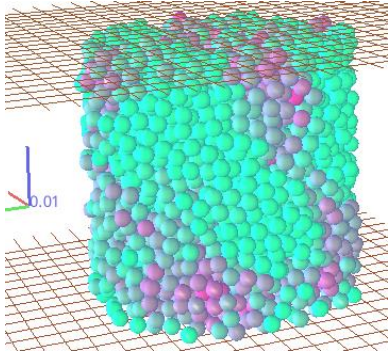
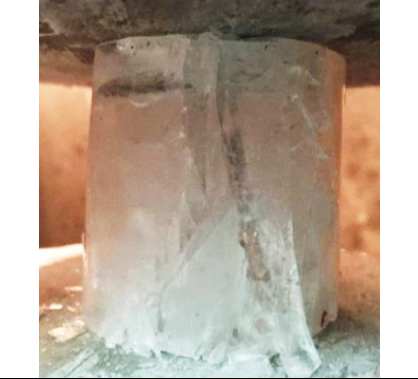
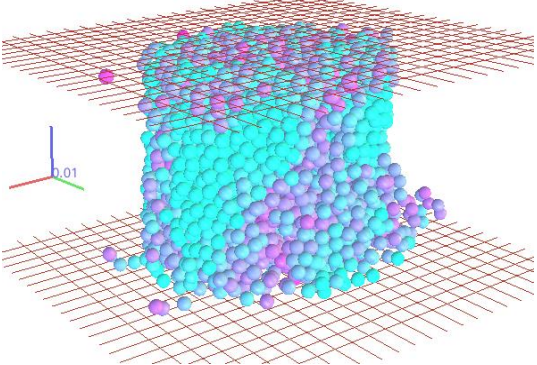

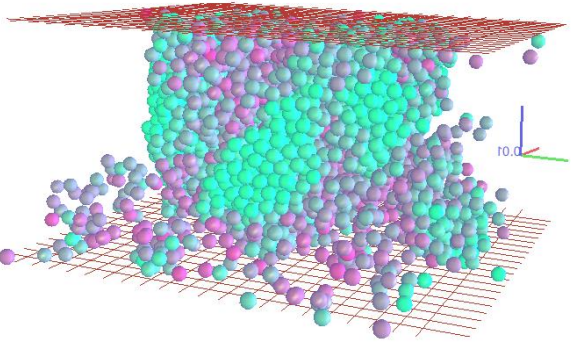
Table 2 contains photographs of a typical experiment and a visualization of the computations performed for the specimen.

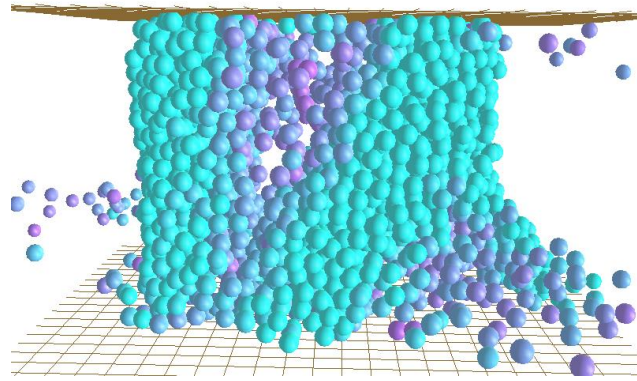
First, small local cracks appear, corresponding to jumps and fluctuations on the stress-strain curve (Fig. 3 up to the strain of ~1.5%). Next, vertical cracks passing through the entire specimen form (Table 2, row 1), they grow and increase in number (Table 2, row 2). After that, some fragments start to break off and separate from each other (Table 2, row 3). The load received by the specimen decreases, and it fractures completely.

Figure 4 shows a visualization of the specimen with a vertical crack. For clarity, the horizontal displacements of the elements are shown at  $\times 100$  magnification, allowing to visualize the cracking in the specimen. The crack is rotated by a small angle from the vertical. Spalling of smaller fragments starts in one region of the specimen.



**Table 2.** Comparison of experimental and computational results for compression of ice specimen

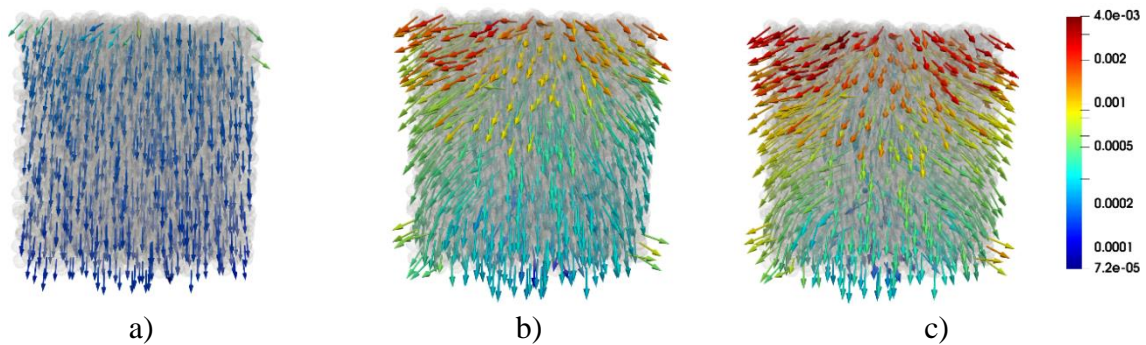
#	Experiment	Simulation
1		
2		
3		
4		



**Fig. 4.** Visualization of crack in the specimen model at  $\times 100$  magnification

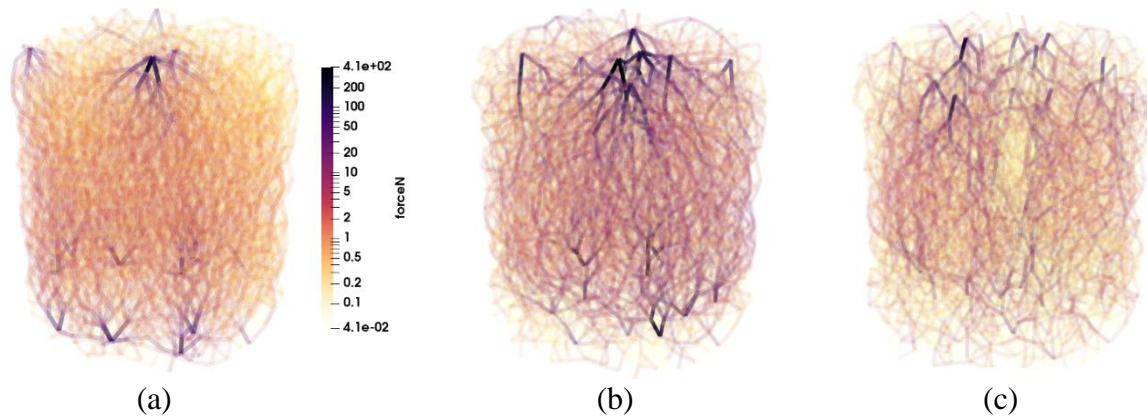
Let us summarize the computed internal factors for various loading stages. The times corresponding to the strain equal to  $\varepsilon = 0.52$ ,  $1.57$  and  $3.66$  % were taken for assessment, which corresponds to the computational steps  $N = 2'000$ ,  $6'000$  and  $14'000$ . The first value corresponds to the initial loading stage, with virtually no damage in the specimen, the second value was taken after the peak of maximum strength was passed, with the main longitudinal cracks formed in the specimen, and the third value lies in the region of residual strength approximately at the level of the first stress value. The scales in the figures are exponential with the same magnification for all loading stages of the corresponding parameter.

Figure 5 shows the displacement vectors of the elements during loading of the specimen. The displacements are insignificant at first, the movement of the elements in one direction corresponds to elastic deformation of the specimen, but with small local effects. At the following stages, the material is squeezed out in different directions, with separation cracks forming.

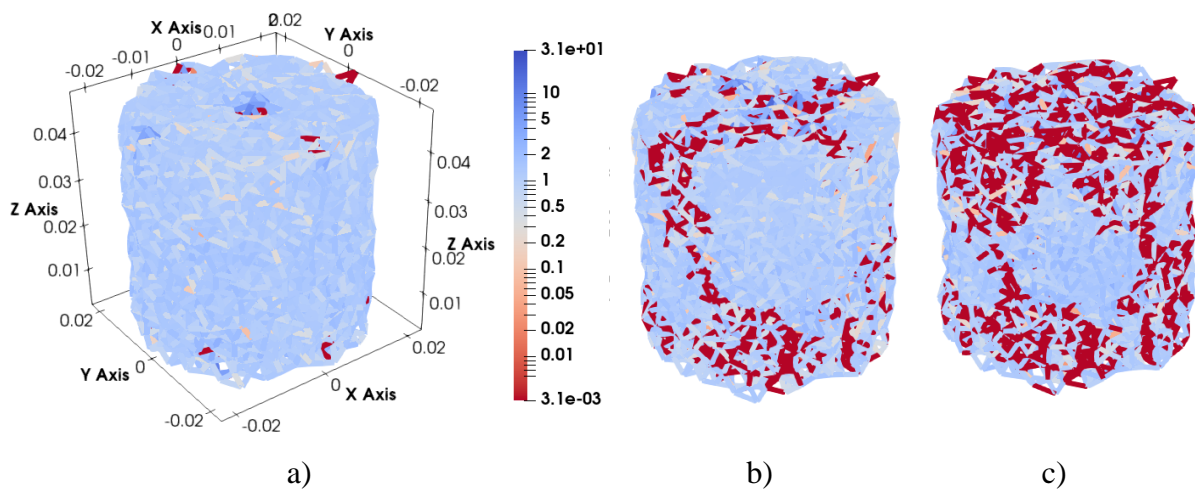


**Fig. 5.** Displacements of elements in the model (m):  
 $\varepsilon = 0.52$  % (a),  $\varepsilon = 1.57$  % (b),  $\varepsilon = 3.66$  % (c)

Figure 6 shows the lines of normal stresses in the element bonds (measured in N). Bonds with low values are shown as semi-transparent for clarity, depending on the level of stress. Because the specimen is randomly and unevenly filled with elements, stress concentration regions are observed, which are distributed in the specimen in a sequence similar to grains in a real material. The specimen in Fig. 6(a) is a unified system with separate concentrators at the boundaries due to the edge effect. As the load increases, the stresses in all bonds increase as well, distributing to the peripheral sections of the grid (Fig. 6(b)). The regions separated by cracks are not visible in the case of normal stresses. Evidently, stress relaxation occurs in the region of residual strength (Fig. 6(c)). The light intermediate regions between the dark ones correspond to the boundaries of the open cracks dividing the specimen.



**Fig. 6.** Normal forces in the bonds between the elements (N):  
 $\varepsilon = 0.52\%$  (a),  $\varepsilon = 1.57\%$  (b),  $\varepsilon = 3.66\%$  (c)



**Fig. 7.** Tangential forces in the bonds between the elements (N):  $\varepsilon = 0.52\%$  (a),  
 $\varepsilon = 1.57\%$  (b),  $\varepsilon = 3.66\%$  (c)

Figure 7 shows the tangential forces in the bonds between the elements. They are much smaller than normal forces.

The zero and near-zero values of tangential forces are colored in red. Regions with broken bonds between elements can be traced from these values, while contact forces are transmitted between elements that are already independent. The fractured specimen breaks into separate fragments representing groups of connected elements.

## Conclusion

We carried out an experimental study of compression in ice specimens, obtaining the stress-strain and strength characteristics of the specimens necessary for comparative analysis of the simulation.

We performed numerical simulation for compressive fracture of ice using the discrete element method. Yade software was used, implementing a model of bonded particles taking into account damage. Using a complex fracture model allows to achieve repetitive brittle fracture as in the experiment with fracture of the specimens.

The simulation carried out for fracture of a hyperboloid-shaped specimen under uniaxial loading allowed to estimate the parameters of the material model. Different behaviors were observed depending on the load: a smooth drop in the load during compression and cracking of the material and abrupt fracture during tension. The tensile and compressive strengths obtained

differed by 3.26 times. Calibration of the model was carried out. The parameters of the element bonds were determined based on experimental data.

We can conclude from the experimental data that the model provides a correct physical description for loading and fracture of the ice specimen. The stress-strain curves show a similar behavior. The level of load and strain is in agreement with the experimental results. The difference between the experimental and computational strains for compression of the ice specimen was about 2 %. The model can be used to predict the behavior of ice under compressive loading.

The model can be further extended to accounting for temperature factors and loading rates. Analysis of behavior of reinforced ice is also a crucial issue. Various types of reinforcement allow to increase the strength and modify the fracture behavior of ice (making it more ductile). However, this problem is far more complicated than simulation of pure ice; solving it could provide further insights into the applications of composite ice materials for infrastructure development in regions with a cold climate.

## References

1. Nuzhnyi GA, Cherepanin RN, Buznik VM, Grinevich DV, Landik DN. Compression Features of Ice Composite Materials with Natural Reinforcing Fillers. *Inorganic Materials: Applied Research*. 2020;11:103-108.
2. Fomin AYu, Shabalin VM. Penetration of steel projectiles through finite thickness ice targets. *Journal of Applied Mechanics and Technical Physics*. 2019;60(3):146-153. (In-Russian)
3. Orlov MY, Glazyrin VP, Orlov YN. Research of the behavior of metal plates subject to ice ball. *Journal of Physics: Conference Series*. 2020;1459(1): 1–14.
4. Bogorodsky VV, Gavrilov VP. *Ice. Physical properties. Modern methods of glaciology*. Leningrad: Gidrometeoizdat Press; 1980. (In-Russian)
5. Potekaev AI, Porvatov GN, Skripnik VV, Skripnyak VA. Physico-mechanical behavior of ice under dynamic loads. *News of Higher Educational Institutions. Physics*. 2021;64(6): 89-94 (In-Russian)
6. Glazova, EG, Krylov SV, Chekmarev DT. Numerical modeling of the impact of an ice sphere on an obstacle. *Scientific Note of Kazan University. Series: Physical and Mathematical Sciences*. 2020;162(2):137-147. (In-Russian)
7. Gerasimov SI, Zubankov AV, Krivosheev OV, Kalmykov AP, Kapinos SA, Gluhov AA, Piseckij VV, Gerasimova RV. Investigation of the penetration of an ice barrier by a cylindrical drummer. *Bulletin of the National Research Nuclear University MEPhI*. 2020;9(2): 95-99. (In-Russian)
8. Zemlyak VL, Vasilyev AS, Kozin VM, Rogozhnikova EG. The influence of the cross-sectional shape of the body on the parameters of flexural-gravity waves during under-ice motion. *Journal of Physics: Conference Series*. 2020;1709: 1-10.
9. Grinevich DV, Buznik VM, Nuzhnyi GA. Review of numerical methods for simulation of the ice deformation and fracture. *Trudy VIAM (Proceedings of VIAM)*. 2020;8(90): 109-122. (In-Russian)
10. Buznik V, Golushko S, Amelina E, Belyaev V, Bryndin L, Gorynin A, Shapeev V. Determining the law of ice deformation. *Journal of Physics: Conference Series*. 2019;1404(012010): 1-7.
11. Nisja HA. *Numerical Modelling of Brittle Failure in Ice Structures. Master thesis*. Norway: Norwegian University of Science and Technology; 2014.
12. Zhang N, Zheng X, Ma Q. Updated Smoothed Particle Hydrodynamics for Simulating Bending and Compression Failure Progress of Ice. *Water*. 2017;9(11): 882.

13. Zhang N, Zheng X, Ma Q, Hu Zh. A numerical study on ice failure process and ice-ship interactions by Smoothed Particle Hydrodynamics. *International Journal of Naval Architecture and Ocean Engineering*. 2019;11(2): 796-808.
14. Alder BJ, Wainwright TE. Phase Transition for a Hard Sphere System. *The Journal of Chemical Physics*. 1957;27(5): 1208–1209.
15. Cundall PA. *The measurement and analysis of accelerations in rock slopes*. PhD thesis. Imperial College London; 1971.
16. Cundall PA. A discrete numerical model for granular assemblies. *Géotechnique*. 1979;29(1): 47–65.
17. *EDEM 2017. User Guide*. Edinburgh, Scotland, UK: DEM Solutions Ltd.; 2016.
18. Kloss Ch, Goniva C, Hager A, Amberger S, Pirker S. Models, algorithms and validation for opensource DEM and CFD-DEM. *Progress in Computational Fluid Dynamics an International Journal*. 2012;12(2/3): 140-152.
19. Weinhart T, Orefice L, Post M, van Schroyensteen Lantman M, Denissen I, Tunuguntla D, Tsang J, Cheng H, Shaheen M, Shi H, Rapino P, Granonio E, Losacco N, Barbosa J, Jing L, Alvarez Naranjo J, Roy S, den Otter W, Thornton A. Fast, flexible particle simulations. Fast, flexible particle simulations - An introduction to MercuryDPM. *Computer Physics Communications*. 2020;249: 1-19.
20. Šmilauer V, Gladky A, Kozicki J, Modenese C, Stránský J. *Using and Programming. Yade Documentation 2nd ed*. The Yade Project; 2015.
21. Fleissner F. *Parallel Object-Oriented Simulation with Lagrangian Particle Methods*. PhD thesis. Universitat Stuttgart; 2010.
22. Šmilauer V. Cohesive Particle Model using the Discrete Element Method on the Yade Platform. PhD thesis, Czech Technical University in Prague. 2010. Available from: <http://tel.archives-ouvertes.fr/docs/00/50/24/02/PDF/thesis.pdf> [Accessed 18th March 2021].
23. Lavrov VV. *Deformation and strength of ice*. Leningrad: Gidrometeoizdat; 1969. (In-Russian)
24. Voitkovsky KF. *Mechanical properties of ice*. Moscow: Publishing house of the Academy of Sciences of the USSR; 1960. (In-Russian)
25. Fish A, Zaretsky Y. *Ice Strength as a Function of Hydrostatic Pressure and Temperature*. Carrel Report; 1997.
26. Jones SJ. The confined compressive strength of polycrystalline ice. *Journal of Glaciology*. 1982;28(98): 171-178.
27. Butyagin IP. *Strength of ice and ice cover*. Novosibirsk: Science. Siberian department; 1966. (In-Russian)
28. Gagnon R, Gammon P. Triaxial experiments on iceberg and glacier ice. *Journal of Glaciology*. 1995;41(139): 528-540.
29. Grinevich DV, Nuzhnyi GA, Buznik VM, Yakovlev NO, Goncharova GY, Razomasov ND. Fracture of reinforced ice composite materials under flexural mechanical loading. *Materials Science*. 2020;1: 18-24. (In-Russian)

## THE AUTHORS

**Grinevich D.V.**   
e-mail: d.v.grinevich@gmail.com

**Nuzhnyi G.A.**  
e-mail: egor\_need@mail.ru

**Buznik V.M.**  
e-mail: bouzник@ngs.ru